J|A|C|S
ARTICLES
Published on Web 02/19/2005

On the Mechanism of Hydrophobic Association of Nanoscopic Solutes

Niharendu Choudhury† and B. Montgomery Pettitt*

Contribution from the Department of Chemistry, University of Houston, Houston, Texas 77204-5641

Received September 24, 2004; E-mail: pettitt@uh.edu

Abstract: The hydration behavior of two planar nanoscopic hydrophobic solutes in liquid water at normal temperature and pressure is investigated by calculating the potential of mean force between them at constant pressure as a function of the solute−solvent interaction potential. The importance of the effect of weak attractive interactions between the solute atoms and the solvent on the hydration behavior is clearly demonstrated. We focus on the underlying mechanism behind the contrasting results obtained in various recent experimental and computational studies on water near hydrophobic solutes. The length scale where crossover from a solvent separated state to the contact pair state occurs is shown to depend on the solute sizes as well as on details of the solute−solvent interaction. We find the mechanism for attractive mean forces between the plates is very different depending on the nature of the solute−solvent interaction which has implications for the mechanism of the hydrophobic effect for biomolecules.

I. Introduction

The role of the hydrophobic effect on the hydration and stability of large macromolecular assemblies in aqueous solution has long been recognized.[1−4] The hydrophobic effect[4−6] is one of the most important driving forces for the formation of the folded, native structure of proteins, formation of micelles, bilayer membranes, and many other biological assemblies in aqueous solution. However, a quantitative understanding of the role of this effect on the association/dissolution of various solutes in aqueous solution remains a problem due to the inherently multiscale nature of the relevant observations.[2] The structure and energetics of the water molecules around small hydrophobic solutes have been well studied.[7−11] Hummer et al.[9] have demonstrated that the probability of spontaneous cavity formation in bulk water can be used to predict the solvation thermodynamics of small hard sphere solutes. Statistical thermodynamic treatments using approximate correlation functions and lattice based models predicted[11] a significant effect on the chemical potential of solvation due to relatively weak van der Waals attractions as a function of size of the solute affecting the resulting surface area and volume contributions. The central issue remaining for biomolecules is the mechanism of the hydrophobic effect.

Recent theoretical works by Chandler and co-workers,[12−15] based on a mesoscopic square gradient theory for the liquid vapor interface, have shown that there is a significant difference in the hydration of large hydrophobic solutes as compared to that of small hydrophobic solutes. They have predicted that there is an appreciable amount of water depletion (drying) between two large model hydrophobic objects on the length scale of around 50 Å, which is in sharp contrast to the hydration of small nonpolar solutes where the solvent separated configuration is observed on the length scale of a few angstroms.[7−11] Although no such water depletion has been observed in various early computer simulation studies of water between both smooth[16] and atomic[17] periodically infinite hydrophobic surfaces, a drying transition between two nanoscopic ellipsoidal solutes with a purely repulsive inverse 12th power potential and a 6−12 potential has however been observed by Berne and co-workers.[18,19] It is not clear to what extent the effects of water models used,[20] and the geometry of the hydrophobic pocket formed due to the ellipsoidal solutes[21] might affect the results. Other cavity geometries also complicate a straightforward interpretation.[22] On the other hand, Hummer et al.,[21] based on a combined study of simulations and perturbation theory, have

† On leave from RC & CD Division, Bhabha Atomic Research Centre, Mumbai 400 085, India.

(1) Kauzmann, W. *Adv. Protein Chem.* **1959**, *14*, 1.
(2) Pratt, L. R.; Pohorille, A. *Chem. Rev.* **2002**, *102*, 2671.
(3) Tanford, C. *The Hydrophobic Effect: Formation of Micelles and Biological Membranes*; John Weiley: New York, 1973.
(4) Dill, K. A. *Biochemistry* **1990**, *29*, 7133.
(5) Tanford, C. *Protein Sci.* **1997**, *6*, 1358.
(6) Tanford, C. *Science* **1978**, *200*, 1012.
(7) Pangali, C.; Rao, M.; Berne, B. J. *J. Chem. Phys.* **1979**, *71*, 2975.
(8) Smith, D. E.; Haymet, A. D. J. *J. Chem. Phys.* **1993**, *98*, 6445.
(9) Hummer, G.; Garde, S.; Garcia, A. E.; Pohorille, A.; Pratt, L. R. *Proc. Natl. Acad. Sci. U.S.A.* **1996**, *93*, 8951.
(10) Southall, N. T.; Dill, K. A. *Biophys. Chem.* **2002**, *101*, 295.
(11) Perkyns, J. S.; Pettitt, B. M. *J. Phys. Chem.* **1996**, *100*, 1323−1329.
(12) Lum, K.; Chandler, D.; Weeks, J. D. *J. Phys. Chem. B* **1999**, *103*, 4570.
(13) Huang, D. M.; Chandler, D. *Proc. Natl. Acad. Sci. U.S.A.* **2000**, *97*, 8324.
(14) Huang, D. M.; Geissler, P. L.; Chandler, D. *J. Phys. Chem. B* **2001**, *105*, 6704.
(15) Huang, D. M.; Chandler, D. *J. Phys. Chem. B* **2002**, *106*, 2047.
(16) Lee, C. Y.; McCammon, J. A.; Rossky, P. J. *J. Chem. Phys.* **1984**, *80*, 4448.
(17) Lee, S. H.; Rossky, P. J. *J. Chem. Phys.* **1994**, *100*, 3334.
(18) Wallqvist, A. Berne, B. J. *J. Phys. Chem.* **1995**, *99*, 2885.
(19) Wallqvist, A. Berne, B. J. *J. Phys. Chem.* **1995**, *99*, 2893.
(20) Huang, X.; Margulis, C. J.; Berne, B. J. *Proc. Natl. Acad. Sci. U.S.A.* **2003**, *100*, 11953.
(21) Hummer, G.; Garde, S. *Phys. Rev. Lett.* **1998**, *80*, 4193.

10.1021/ja0441817 CCC: $30.25

observed only a very weak dewetting near a large spherical hard sphere solute−water interface.

However, some interesting observations made in recent computational studies[23,24] on the behavior of water inside an atomistically modeled carbon nanotube (CNT) made up of a curved hydrophobic graphite sheet have further renewed the interests in the hydration of large hydrophobic objects. Even though the pore is completely enclosed by hydrophobic carbon atoms and narrow enough to accommodate just a single strand of water molecules, they have observed the water molecules inside the tube in the form of a one-dimensional hydrogen-bonded chain. A significant layering of water molecules adjacent to the outer periphery of the carbon nanotube has also been observed. With a reduced attractive interaction; however, a sharp two-state transition between filled and empty states of the nanotube interior on the nanosecond time scale was observed.[23,25] Given the conventional wisdom, it is surprising to see that a one-dimensional system of water molecules can exist in the hydrophobic pore, where there is a considerable loss of hydrogen bonding compared to bulk. The stability of the one-dimensional chain of water inside the CNT has been explained in terms of binding energy distribution of water molecules. As argued, although there are on an average around four hydrogen bonds per water molecule in the bulk water as compared to two inside CNT, there are considerable fluctuations in the number of hydrogen bonds in bulk water, which means that a significant fraction of water in the bulk are incompletely hydrogen bonded and thus have less binding energy. While inside the nanotube, water molecules are shielded from such fluctuations, and thus this class of molecules with low binding energy is not present.[24] It was argued[23] that the binding energy for the bulk water has broader distribution that includes both low energy and high energy states, whereas, in CNTs, although low energy states are less populated, a sharp and strong distribution around moderate energy compensates for the loss of these low energy states and, thus, provides enough favorable difference in the excess chemical potential that helps water to enter inside the CNT.

The results from this study are in sharp contrast from the usual notion that water might be expelled from the narrow hydrophobic pore[22] and also seems to contradict the simulation results of Berne and co-workers,[18,19] which dealt with water simulations between two hydrophobic ellipsoids. They found a sharp dewetting transition when the separation between the two plates becomes slightly less than two molecular diameters. Those authors did not observe any monolayer state between the two hydrophobic surfaces. The potential of mean force (PMF) between the two ellipsoids with repulsive interaction has been shown to be strikingly different at a smaller separation from the same between two small hydrophobic solutes such as methane in water. In a region where the interplate distance is less than 9.5 Å, although one or two water layers can easily fit between the two ellipsoidal solutes, all the waters are expelled completely giving rise to a sharp decrease in the PMF. This investigation was restricted to separations between the two ellipsoid in the range 5 to 15 Å. Another study at this length scale but using infinite smooth walls by Forsman et al.[26] reports no cavitation, although they observed a depression of the density in the interwall region. A similar observation was made some time ago by Luzar et al.[27] using a grand canonical Monte Carlo simulation of a simplified waterlike model between two smooth hard infinite walls. Dynamics of evaporation of water confined in hydrophobic pores have also been explored in a number of lattice gas simulation studies,[28] and in a recent atomistic simulation study,[29] barrier height and rate of evaporation of confined water were calculated on the basis of a discrete lattice representation of the cavity volume as the reaction coordinate.

The need for further studies on the behavior of water near hydrophobic material also stems from the recent experimental observations,[30,31] which indicate that water may wet the graphite surface and therefore may act as a lubricant between two layers of graphite. This is a well-known phenomena for diatomic gases and other intercalators.[32] While a number of surface force measurement experiments[33−35] were consistent with cavitation between nonpolar surfaces, others observed[36−38] the persistent presence of water between two such surfaces. A number of recent experimental investigations[39−42] indicating contrasting results on the wetting/dewetting of large hydrophobic surfaces by water and subsequent recent discussion[43] on this issue demonstrate a growing interest on the subject. Some of the recent computational studies[26,44,45] have been aimed at elucidating the microscopic mechanism behind the strong attractive interaction between two large plates observed in some surface force measurements.[36−38,46] It is worth mentioning that the attractive force, as observed in the meso to macroscopic surface force experiments are fairly long ranged and may extend over several thousands of angstroms in some experiments[38] to a few hundred angstroms in some others.[47] It is very difficult currently to study such long ranged forces in a microscopic (molecular) simulation. Attempts[44,45] have been made to simulate such systems in the intermediate length scales extending over a few tens of angstroms. Results from these simulations, however, cannot be used to explain the very long ranged attractive

(22) Walqvist, A.; Gallicchio, E.; Levy, R. M. *J. Phys. Chem.* **2001**, *105*, 6745−6753.
(23) Hummer, G.; Rasaiah, J. C.; Noworyta, J. P. *Nature* **2001**, *414*, 188.
(24) Sansom, M. S. P.; Biggin, P. C. *Nature* **2001**, *414*, 156.
(25) Waghe A.; Rasaiah, J. C.; Noworyta, J. P.; Hummer, G. *J. Chem. Phys.* **2002**, *117*, 10789.
(26) Forsman, J.; Jonsson, B.; Woodward, C. E. *J. Phys. Chem.* **1996**, *100*, 15005.
(27) Luzar, A.; Bratko, D.; Blum, L. *J. Chem. Phys.* **1987**, *86*, 2955.
(28) Lum, K.; Luzar, A. *Phys. Rev. E* **1997**, *56*, R6283. Luzar, A.; Leung, K. *J. Chem. Phys.* **2000**, *113*, 5836. Leung. K.; Luzar, A. *J. Chem. Phys.* **2000**, *113*, 5845.
(29) Leung, K.; Luzar, A.; Bratko, D. *Phys. Rev. Lett.* **2003**, *90*, 065502.
(30) Schrader, M. E. *J. Phys. Chem.* **1980**, *84*, 2774.
(31) Luna, M.; Colchero, J.; Baro, A. M. *J. Phys. Chem. B* **1999**, *103*, 9576.
(32) Chen, Z. M.; Karim, O. A.; Pettitt, B. M. *J. Chem. Phys.* **1988**, *89*, 1042−1048.
(33) Yaminsky, V. V.; Yushchenko, V. S.; Amelina, E. A.; Shchukin, J. *J. Colloid Interface Sci.* **1983**, *96*, 301.
(34) Yushchenko, V. S.; Yaminsky, V. V.; Shchukin, E. D. *J. Colloid Interface Sci.* **1983**, *96*, 307.
(35) Yaminsky, V. V.; Amelina, E. A.; Shchukin, E. D. *Colloids Surf.* **1983**, *6*, 68.
(36) Claesson, P. M.; Christenson, H. K. *Science* **1988**, *239*, 390.
(37) Christenson, H. K. In *Modern Approaches to wettability: Theory and Applications*; Schrader, M. E., Loeb, G., Eds.; Plenum: New York, 1992.
(38) Parker, J. L.; Claesson, P. M.; Attard, P. *J. Phys. Chem.* **1994**, *98*, 8464.
(39) Steitz, R.; Gutberlet, T.; Hauss, T.; Klosgen, B.; Krastev, R.; Schemmel, S.; Simonsen, A. C.; Findenegg, G. H. *Langmuir* **2003**, *19*, 2409.
(40) Jensen, T. R.; Jensen, M. O.; Reitzel, N.; Balashev, K.; Peters, G. H.; Kjaer, K.; Bjornholm, T. *Phys. Rev. Lett.* **2003**, *90*, 086101.
(41) Schwendel, D.; Hayashi, T.; Dahint, R.; Pertsin, A.; Grunze, M.; Steitz, R.; Schreiber, F. *Langmuir* **2003**, *19*, 2284.
(42) Yaminsky, V.; Ohnishi, S. *Langmuir* **2003**, *19*, 1970.
(43) Ball, P. *Nature* **2003**, *423*, 25.
(44) Bratko, D.; Curtis, R. A.; Blanch, H. W.; Prausnitz, J. M. *J. Chem. Phys.* **2001**, *115*, 3873.
(45) Hayashi, T.; Pertsin, A. J.; Grunze, M. *J. Chem. Phys.* **2002**, *117*, 6171.
(46) Pashley, R. M.; McGuiggan, P. M.; Ninham, B. W.; Evans, D. F. *Science* **1985**, *229*, 1088.
(47) Wood, J.; Sharma, R. *Langmuir* **1995**, *11*, 4797.

solvation force extending over thousands of angstroms, as indicated in the experiments. In most of these computational studies, the plates are modeled as idealized smooth structureless walls with either hard sphere or an integrated van der Waals' type wall−water interactions and thus lack details relevant for a study of the cumulative effect of attractive solute−solvent interactions on the potential of mean force between the plates.

Some recent studies[48−50] have also focused on the interaction of water with the carbon atoms of carbon nanotubes or graphite sheets. Molecular dynamics simulations of water droplets on graphite sheets[49] have been performed to study the effect of the potential parameters on the contact angle of the droplet. An empirical linear relationship between contact angle and water monomer binding energy has been established, and new potential parameters for the carbon−water interaction have been suggested. A very recent investigation of Berne and co-workers[20] on the dewetting induced collapse of two ellipsoidal hydrophobic particles interacting with the Gay−Berne potential and a similar result for nanotubes in water[50] has further focused interest on the issue of hydrophobic hydration of large solutes. Berne and co-workers[20] have found dewetting between two repulsive ellipsoidal solutes at a critical distance of around 14 Å. However, using a different slightly attractive solute−water interaction potential, they have found the critical distance at which dewetting occurs to decrease to ∼10 Å. This observation calls into question the role the attractive interactions between the large number of solute atoms and water could play on the dewetting phenomena. Given the magnitude of attractions for systems with heteroatoms, the range of the relevant phenomena is critical to its role in protein folding and association. Although effects of attractive solute−solvent interactions on the hydration water structure around spherical solutes have been studied,[15,51] conclusions from such studies still show contradictions. In one such study, using planar averaged attractive solute−solvent attractions, Huang et al.[15] have shown that effect of attraction is too small to alter the conclusions of their earlier findings on dewetting induced hydrophobic association and entropies of protein unfolding, which is based on hard sphere solvation.[13] On the other hand, in another study[51] of methane cluster solvation, it was shown that large methane clusters with realistic dispersion interaction have a higher contact water density as compared to bulk, while the hard sphere analogue of the same size cluster shows a density depression. However, no detailed study about the effect of attractions on the spontaneous cavity formation between two such hydrophobic clusters that forms the basis of dewetting induced collapse or aggregation of hydrophobic solutes was considered. In fact, the consequences on the mechanism of the hydrophobic effect in terms of free energy change have not been fully examined.

Despite the large number of investigations, a consensus and unified view of hydrophobic hydration of large solutes has not emerged,[43] and many mechanistic issues still remain unresolved. In fact, the reason behind the differences in the results from some simulation studies[23,24,48,49] that report wetting with those from some others[18−20,50] that point to dewetting or cavitation between two large solutes is not clear so far.

We have chosen a computationally intensive but reliable method for understanding the solvation thermodynamics of nanoscopic, planar, apolar solutes in water by calculating the potential of mean force (PMF) between the solute molecules. Although there are some recent investigations on water behavior in and around large hydrophobic objects, to the best of our knowledge, very few simulations[18,19,50] so far have reported the potential of mean force between two large or nanoscopic hydrophobic solutes. However, these simulation studies have not systematically addressed issues regarding the choice of the solute size and the nature of the solute−solvent interaction on the dewetting induced aggregation of hydrophobic solutes.

In the present study we have therefore made an effort to address issues related to attraction and size of the solute through a number of all atom, constant pressure, molecular dynamics simulations of two nanoscopic graphitelike plates in water. We have calculated the potential of mean force between two plates for two different kinds of solute−solvent interactions. We include an analysis of the density distributions and orientational and hydrogen bond profiles to obtain the differences in mechanisms in the two cases. In addition, simulation runs have been performed with varying degrees of solute−solvent attractions to investigate the stability of the first solvent separated state, which is not found in many recent simulations with either purely repulsive or planar averaged weakly attractive solute−solvent interactions. The stability of the monolayer between two solutes for attractive solute−solvent interaction rests on a fine balance between hydrogen bonding energy and solute−solvent attractive interaction.

II. Method

In the present work, we have studied the behavior of systems where water is around and often between two, large, flat hydrophobic solutes. The water molecule was represented by the standard SPC/E[52] model, and each of the hydrophobic solutes considered here was modeled as a graphitelike sheet or plate placed in a flat, hexagonal lattice with carbon−carbon bond lengths of 1.4 Å. The main solutes for our study have 60 carbon atoms each with dimensions of ∼11 Å × 12 Å. Some limited studies with systems with 28 and 180 atoms in each plate were also performed. The two sheets were placed symmetrically around the center of a cubic box containing water molecules (1800 for the 60 atom solutes), with the plates being parallel to each other as well as to the *xy*-plane with a fixed intersolute distance r_0. The overlapping water molecules from the immediate vicinity of the two plates were removed followed by a steepest decent minimization. The carbon atoms of the solute were modeled as uncharged particles interacting with Lennard−Jones (LJ) potential with diameter $\sigma_{CC} = 3.4$ Å and well depth $\epsilon_{CC} = 0.086$ kcal mol $^{-1}$ (or 0.3598 kJ mol^{-1}), corresponding to the sp^2 carbon atoms in the AMBER 96 force field,[53] the same used by Hummer et al.[23] Hereafter this model solute is referred to as the type I solute. To examine the effects of solute−solvent attraction on the result, we also considered a purely repulsive interaction potential for the carbon atoms of the graphite plates with water. In this case, the solute was geometrically the same as type I solute but the solute−water interaction potential was represented by the repulsive part of the

(48) Walther, J. H.; Jaffe, R.; Halicioglu, T.; Koumoutsakos, P. *J. Phys. Chem. B* **2001**, *105*, 9980.
(49) Werder, T.; Walther, J. H.; Jaffe, R. L.; Halicoioglu, T.; Koumoutsakos, P. *J. Phys. Chem. B* **2003**, *107*, 1345.
(50) Walther, J. H.; Jaffe, R. L.; Kotsalis, E. M.; Werder, T.; Halicioglu, T.; Koumoutsakos, P. *Carbon* **2004**, *42*, 1185−1194.
(51) Ashbaugh, H. S.; Paulaitis M. E. *J. Am. Chem. Soc.* **2001**, *123*, 10721−10728.
(52) Berendsen, H. J. C.; Grigera, J. R.; Straatsma, T. P. *J. Phys. Chem. B* **1987**, *91*, 6269.
(53) Cornell, D. W.; Cornell, W. D.; Cieplak, P.; Bayly, C. I.; Gould, I. R.; Merz, K. M.; Ferguson, D. M.; Spellmeyer, D. C.; Fox, T.; Caldwell, J. W.; Kollman, P. A. *J. Am. Chem. Soc.* **1995**, *117*, 5179.

LJ potential according to the Weeks−Chandler−Anderson (WCA)[54] decomposition scheme; i.e.

$$u(r) = 4\epsilon\left[\left(\frac{\sigma}{r}\right)^{12} - \left(\frac{\sigma}{r}\right)^{6}\right] + \epsilon, \text{ for } r < r_m$$
$$= 0, \text{ for } r \geq r_m \quad (1)$$

where $r_m = 2^{1/6}\sigma$ is the distance at which the LJ potential has a minimum. The symbols σ and ϵ in the above equation refer to the usual size and energy parameters σ_{CC} and ϵ_{CC} of the solute atoms in the case of solute−solute interaction and σ_{OC} and ϵ_{OC} in the case of solute−water interaction. This model of solute with the repulsive interaction potential will be referred to as a type II solute below. In both of the cases usual Lorentz−Berthelot mixing rules [$\sigma_{OC} = (\sigma_{CC} + \sigma_{OO})/2$ and $\epsilon_{OC} = (\epsilon_{CC}\epsilon_{OO})^{1/2}$, with σ_{OO} and ϵ_{OO} being the LJ parameters for oxygen atoms of SPC/E water] were employed to calculate the interaction parameters for solute−water LJ interactions. The solutes were kept fixed at a specific intersolute separation r_0. Simulations in the isothermal isobaric (NPT) ensemble were carried out using the molecular dynamics (MD) extended system approach of Nose and Anderson.[55−57] Periodic boundary conditions were applied, and electrostatic interactions were calculated using the Ewald method.[58] The bonds and angles between oxygen and hydrogen atoms of the water molecules were constrained by use of the RATTLE algorithm,[58,59] and the solutes were rigid. All the systems were simulated at a target pressure of 1 atm and a target temperature of 298 K. The equations of motion were integrated using a velocity Verlet algorithm[58,60] with a 2 fs time step.

The potential of mean force between the two solutes as a function of the intersolute separation r_0 was constructed from the free energy differences obtained from a stratified set of simulations with various r_0 values spanning the entire range of interest. In a particular simulation with a fixed r_0, the free energy difference between the r_0 state and a slightly perturbed state, say $r_1(= r_0 \pm dr_0)$, can be calculated using thermodynamic perturbation theory originally due to Zwanzig.[61] The change in Gibbs free energy between the two systems r_0 and r_1 containing N particles, at a specified temperature T and pressure P, is then given by

$$\Delta G = G(r_1) - G(r_0) = -k_B T \ln\langle e^{-[U(r_1)-U(r_0)]/k_B T}\rangle_0 \quad (2)$$

where k_B is the Boltzmann's constant and U denotes the potential energy of the system. The brackets indicate an ensemble average of the enclosed quantity, and the subscript 0 denotes that the average is taken in the reference r_0 state. The value of dr_0 was chosen in such a way that twice its value gave the difference in the interplate separations between two consecutive r_0 values thus employing double wide sampling. Thus, for each reference state (r_0), we have two free energy differences, one involving dr_0 larger and another dr_0 smaller than the reference state r_0. If we use a discrete variable λ_i to represent all the r_0's considered here such that the lowest value of λ_i is zero corresponding to the smallest value of r_0 (say r_0^{min}) and the largest value of λ_i is 1 corresponding to the largest value of r_0 (say r_0^{max}), various interplate separations used in the simulations can be expressed as

$$r_0(\lambda_i) = r_0^{min} + \lambda_i(r_0^{max} - r_0^{min}) \quad (3)$$

For N separate simulations with various λ_i values, using the perturbation technique, we have $2N$ free energy differences ΔG_i and the total PMF $w(r)$ can be constructed from these individual points by connecting them sequentially. The $w(r)$ thus obtained contains an undetermined additive constant, because only the relative free energies between windows are obtained in this approach. To evaluate this constant, we assumed that the $w(r)$ is zero at the largest separation considered. One can express $w(r)$ in terms of $\Delta G_i(r)$ as[62]

$$w[(r(\lambda_i))] = \sum_{j=i}^{2N} \Delta G_j \quad (4)$$

The difference between the full $w(r)$ and the solute−solute potential, $U_{g-g}(r)$, is the solvent induced contribution to the potential of mean force or cavity potential of mean force, $w_{sol}(r)$.

$$w(r) = w_{sol}(r) + U_{g-g}(r) \quad (5)$$

Because of the nature of the Lennard−Jones model, $U_{g-g}(r)$ is expected to be small for all but close configurations. The statistical error of the individual ΔG given by eq 2 is estimated by the standard deviation $\sigma(\Delta G_i)$ from the block averaging procedure defined as[62]

$$\sigma^2(\Delta G_i) = \frac{1}{n_b(n_b - 1)}\sum_{b=1}^{n_b}(\Delta G_{i,b} - \Delta G_i)^2 \quad (6)$$

where n_b is the total number of blocks, $\Delta G_{i,b}$ is the block averaged quantity for the block b and state i. The mean is calculated as an average over all r points; i.e., $1/N\Sigma_{i=1}^{2N}\sigma(\Delta G_i)$. The error $\sigma(w(r))$ on the PMF curve is calculated by propagation of errors of the connecting points.[18,19,62]

Thus, in the present study we have calculated PMFs for two kinds of systems, one involving solute carbon atoms with standard Lennard−Jones interactions corresponding to the sp^2 carbon atom of the AMBER 96 force field[23,53] (type I) and another involving solute carbon atoms with a purely repulsive interaction (type II). In the case of type I solute PMFs, we have performed 52 separate simulation runs corresponding to 52 r_0 (or λ_i) values with $r_0^{min} = 3.0$ Å and $r_0^{max} = 13.2$ Å. Each of these reference states was equilibrated for at least 100 ps, and averages for the PMF were taken over 100 ps of simulation after equilibration. In the case of type II solutes, 64 separate simulation runs with different λ_i values with $r_0^{min} = 3.0$ Å and $r_0^{max} = 15.6$ Å were used to construct the PMF. Each of these reference states was equilibrated for 50 ps followed by an averaging over another 50 ps. In some of the states near first solvent separated configuration, longer runs were required for equilibration.

To study the spatial and orientational structure of the water molecules in and around the two solutes, we have calculated the density profiles and two distributions related to the angles formed by dipole moment and OH bond vectors of the water molecules with a specific direction. To quantify the loss of hydrogen bonds due to geometric confinement, we have calculated hydrogen bond (H-bond) density profiles. A standard geometric criteria[63,64] where two water molecules are considered to be H-bonded only if the inter-oxygen distance is less than 3.5 Å and simultaneously the hydrogen−oxygen (H-bonded) distance is less than 2.45 Å and the H−O···O angle is less than 30° was used. The number density profile, hydrogen bond density profile, and two angular distributions were calculated by considering those water molecules which are inside the rectangular slab with dimensions the same as those of the two plates. For all these calculations additional 300 ps simulations were carried out after the runs for PMF averaging. The spatial and orientational distribution functions in both of the cases were calculated from the coordinates saved at every 0.1 ps over the entire 400 ps.

(54) Chandler, D.; Weeks, J. D.; Andersen, H. C. *Science* **1983**, *220*, 787.
(55) Nose, S. *Mol. Phys.* **2002**, *100*, 191.
(56) Andersen, H. C. *J. Chem. Phys.* **1980**, *72*, 2 384.
(57) Nose, S.; Klein, M. L. *Mol. Phys.* **1983**, *50*, 1055.
(58) Allen, M. P.; Tildesley, D. J. *Computer Simulation of Liquids*; Oxford University, New York, 1987.
(59) Andersen, H. C. *J. Comput. Phys.* **1983**, *52*, 24.
(60) Swope, W. C.; Andersen, H. C.; Berens, P. H.; Wilson, K. R. *J. Chem. Phys.* **1982**, *76*, 637.
(61) Zwanzig, R. W. *J. Chem. Phys.* **1954**, *22*, 1420.
(62) Linse, P. *J. Am. Chem. Soc.* **1993**, *115*, 8793.
(63) Jedlovszky, P.; Brodholt, J. P.; Bruni, F.; Ricci, M. A.; Soper, A. K. Vallauri, R. *J. Chem. Phys.* **1998**, *108*, 8528.
(64) Chandra, A. *Phys. Rev. Lett.* **2000**, *85*, 768.

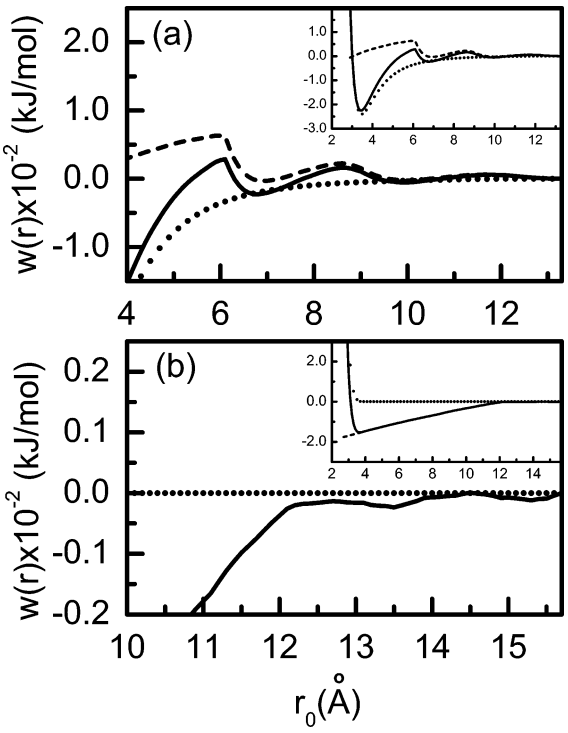

Figure 1. Solute−solute potential contribution $U_{g-g}(r)$ (dotted line) and solvent contribution $w_{sol}(r)$ (dashed line) to the potential of mean force (solid line) for (a) type I solute−water system and (b) for type II solute−water system. The inset in each figure shows the same over the entire range of r_0.

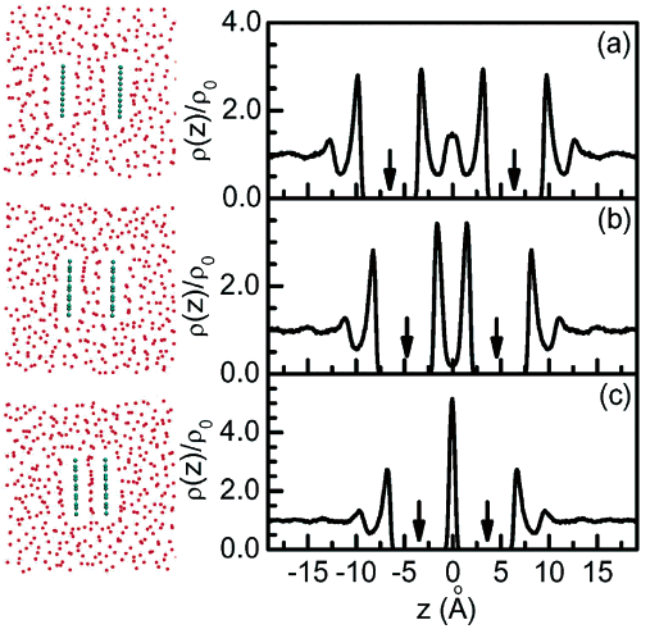

Figure 2. Type I solute−solvent distributions. (Left) Plot of a configuration for the system with type I solutes with the interplate separations (top) $r_0 = 13$ Å, (middle) $r_0 = 9.8$ Å, and (bottom) $r_0 = 6.8$ Å. Red circles are the positions of the water oxygen atoms, and blue circles are the carbon atoms on the solute plates for a slab through the sample. (Right) Plot of the normalized single particle density $\rho(z)/\rho_0$ as a function of z, the distance perpendicular to the plates, corresponding to the systems on the left. In all the density plots two arrows on the x-axis have been drawn to indicate the position (z-coordinate) of the two plates.

III. Results and Discussions

A. Potentials of Mean Force and Spatial Distribution of Water. The potential of mean force, $w(r)$, as a function of the separation between the two large (60 atoms) parallel plates of type I is shown in Figure 1a, and type II, in b along with the solvent induced contribution $w_{sol}(r)$ and the solute−solute potential U_{gg}. The difference in mechanism is striking. For the attractive plates (type I) we find a small solvent stabilization near contact with the overall PMF dominated by the solute−solute attractive potential. For the repulsive solute−solvent system (type II) we find a large, purely solvent induced stabilization near contact.

I. Type I System. For the type I system well outside of contact, Figure 1a shows a shallow minimum in the PMF at a separation of around 13 Å. To visualize the solvent structure near the solute plates, we have shown on the left of Figure 2 the coordinates (single configuration) and on the right the number density profile corresponding to this minimum in the PMF. Three distinct layers of water oxygen in the coordinates and the three well-defined peaks in the density profile corresponding to these water layers indicate around three intervening water layers at this separation.

The strong density peaks just outside the two plates (facing the bulk) also indicate strong layering of water molecules adjacent to the outside surface of the hydrophobic plates. As the distance between the two solutes is reduced, a repulsive free energy change is observed, and at a value of $r_0 = 9.8$ Å, one layer of water is effectively expelled from the region between the two plates leading to another local minimum in PMF. The plot of coordinates and density profile (see middle panels of Figure 2) corresponding to this minimum show a solute−solvent configuration with two intervening water layers. A further reduction in the interplate separation leads to the expulsion of one more layer of water between the two plates at $r_0 = 6.8$ Å, leading to a situation where only a monolayer of water molecules exists in between. This is also supported by the appearance of a sharp peak in the density profile at the middle of the two plates and a single layer of water seen in the coordinates (see the bottom panels of Figure 2, respectively). This feature persisted after continuing the simulation for over 5 ns at this separation.

To visualize the instantaneous change in the number of water molecules ($n(t)$) in the confined region between the two plates, we have calculated $n(t)$ over the period of 5 ns at $r_0 = 6.8$ Å as shown in Figure 3. The plot is reminiscent of dynamic number fluctuations in a grand canonical system.[65] There is no significant change or drift in the number of water molecules $n(t)$ over the entire period of time for $r_0 = 6.8$ Å which is an indication of equilibrium in a grand canonical, dynamic system.[65]

It is important to note that, in the earlier study[19] of PMF between two purely repulsive ellipsoidal solute molecules, no monolayer of water was observed between them. They found a complete expulsion of two water layers as the separation between the two solutes is reduced below 9.5 Å, leading to a drying transition or cavitation. In more recent ellipsoidal solute studies including an attractive potential[20] cavitation between the two ellipses at a separation that could easily fit, a single layer of water was found, leading to a dynamic collapse of the distance between the two solutes. In our present study with the solutes modeled as planar sheets of sp^2 carbon atoms represented by a standard force field, we do not observe any such drying or

(65) Ji, J.; Çağın, T.; Pettitt, B. M. *J. Chem. Phys.* **1992**, *96*, 1333−1342.

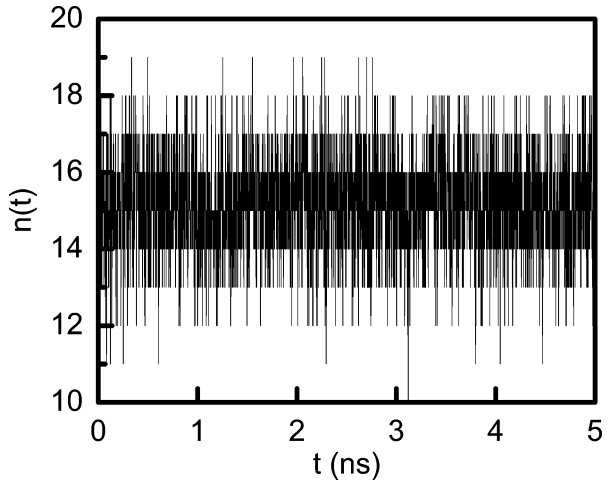

Figure 3. Plot of the number of confined water molecules $n(t)$ between the two plates vs time in nanoseconds for the system corresponding to the bottom part of Figure 2.

cavitation. There is a substantial free energy minimum with large barriers due to solvent induced destabilization on both sides. This result for our type I model is consistent with the recent simulation study of Hummer et al.[23] on the water behavior in a CNT. Using the same AMBER 96 force field for the carbon atoms of the nanotube, they have observed a chain of water molecules inside the nanotube. The radial density plot in their study [see Figure 2b of ref 23] also shows a sharp peak at the middle of the nanotube with enhancement of the water density in the immediate vicinity of the outside wall.

To check the effect of the strength of attractive interactions on wetting, we have also simulated three additional systems with the same size and geometry but different energy parameters, viz., $\epsilon_{CC} = 0.2177$, 0.1512, 0.125 kJ/mol for the nonbonded carbon−carbon LJ interactions. During 500 ps runs of all these cases we observe no dewetting. It is important to mention at this point that the energy parameters for van der Waals (LJ) interaction for the hydrophobic groups relevant to a biomacromolecule such as methyl, ethyl, benzyl, etc., as used in most of the modern force fields, lie within this regime. Thus, the present results should have more relevance to the aggregation−dissociation phenomena of biomacromolecules as compared to the same obtained from a purely repulsive or planar-averaged weakly attractive model system that does not take into account the atomistic nature of the solutes with dispersion interactions.

Between a separation of 6.8−6.2 Å, we observe a significant barrier in the PMF for our type I system; beneath that distance the water model is sterically no longer allowed which leads to a monotonic decrease in the cavity-PMF from that point on. The presence of a soft cusp in $w(r)$ in Figure 1a is coincident with the steric drying. The plots of the coordinates and the density of the system at $r_0 = 6.2$ indicate a layer of water molecules at the confined region, while for $r_0 = 6.0$ Å as shown in Figure 4 no water molecules are found in this region. A 2.5 ns simulation run at $r_0 = 6.2$ Å reveals that the number of water molecules confined between the two plates fluctuates around 14 for most of the simulation time. Although once in that period a large fluctuation made the confined region empty for around 30 ps, water molecules again entered the region and within 100 ps the number of water molecules reached around 14 where it remained with smaller fluctuations. To investigate

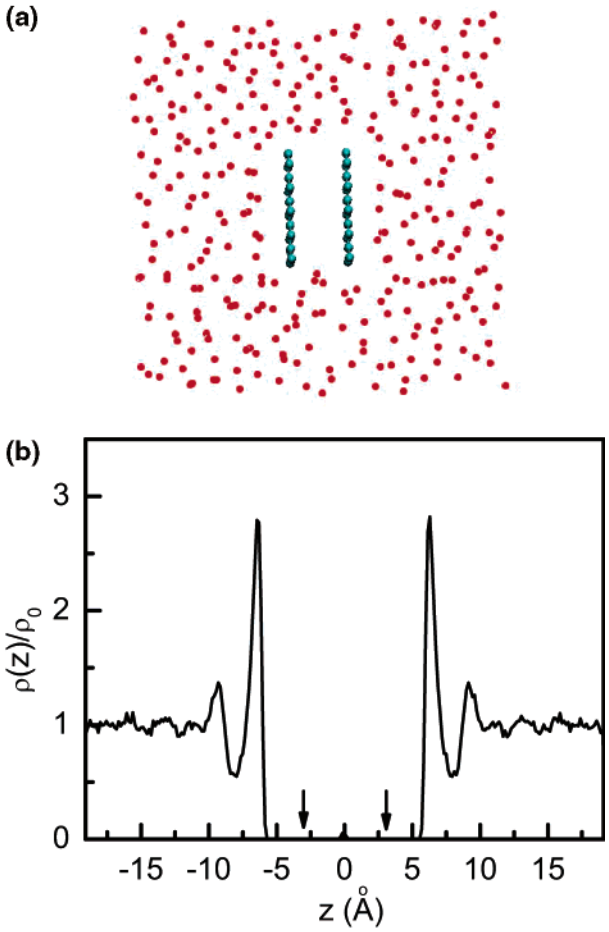

Figure 4. (a) Plot of the coordinates similar to those of Figure 2 but with interplate separation of 6.0 Å. The region between the two plates is completely empty. (b) Plot of the normalized single particle density $\rho(z)/\rho_0$ as a function of z corresponding to the system in Figure 4a.

whether the solute−solvent configuration corresponding to the barrier observed in the solvent induced PMF at $r_0 = 6.2$ is metastable, we also started a simulation at this r_0 from a dry initial state where the interplate region is initially empty. A 1.2 ns simulation shows that the empty cavity is filled by around 14 water molecules within 120 ps, and there after the average number of water molecules remains same. At around $r_0 = 3.5$ Å (see inset of Figure 1a) we observe a contact minimum dominated by the direct potential.

Thus, the PMF between two large hydrophobic solutes with weak attractive forces for the solvent is not dissimilar to that between two small nonpolar solutes involving usual contact pair and solvent separated states.[7−10] Beyond the first solvent separated state at $r_0 = 6.8$, we observed locally stable solvent separated configurations roughly corresponding to integral numbers of layers of water molecules between the two large solutes. The layering of the water molecules around the plates provides a means for accommodating such large hydrophobic objects in water. The estimated mean error[18,19,62] in the PMF per point is around 0.22 kJ/mol, and the propagated error on the free energy or PMF curve is estimated at worst as 2.5 kJ/mol out of a few hundred kJ/mol.

The other properties of the system such as average volume and potential energy of water−water and water−solute interactions as listed in Table 1 undergo only small changes from

Table 1. Properties of the Type I Systems at Various Intersolute Separations at 300 K and 1 atm

r_0 (Å)	vol[a] (nm^3)	U_{SW}[a] (10^2 kJ/mol)[2]	U_{WW}[c] (kJ/mol)	U_{conf}[d] (kJ/mol)
13.0	56.2	−514.64	−45.48	−136.3
12.6	56.2	−510.21	−45.50	−132.7
12.2	56.2	−507.62	−45.48	−131.7
11.8	56.2	−505.21	−45.47	−130.9
11.4	56.2	−501.98	−45.52	−125.5
11.0	56.2	−503.37	−45.49	−129.2
10.6	56.2	−505.87	−45.50	−132.9
10.2	56.1	−518.60	−45.53	−141.3
9.8	56.2	−520.64	−45.52	−146.0
9.4	56.2	−515.94	−45.49	−142.2
9.0	56.2	−496.60	−45.46	−124.8
8.6	56.3	−475.68	−45.48	−107.6
8.2	56.2	−481.63	−45.48	−110.5
7.8	56.2	−491.58	−45.48	−121.7
7.4	56.2	−507.43	−45.46	−133.3
7.0	56.1	−527.17	−45.48	−148.9
6.8	56.3	−524.35	−45.47	−147.9
6.6	56.1	−524.28	−45.47	−147.6
6.2	56.3	−486.91	−45.43	−117.0
6.0	56.7	−352.27	−45.48	
5.8	56.7	−340.18	−45.50	-

[a] Volume of the simulation box. [b] U_{SW} is the solute−water potential energy. [c] U_{WW} is the water−water potential energy. [d] U_{conf} is the potential energy of the solute with water molecules in the confined region.

13.2 to 6.2 Å. Below this point all the water molecules are expelled from the confined region and moved to the bulk, and at constant pressure, the system responds to this by slightly increasing the overall volume of the box. The increase in average volume of around 0.4 nm^3 in going from an $r_0 = 6.2$ Å to $r_0 = 6.0$ Å state is consistent with the volume of around 14 water molecules (which were confined at $r_0 = 6.2$ Å and released to the bulk at $r_0 = 6.0$ Å) corresponding to the bulk density of water. Thus, the total volume accessible to the water molecules remains unchanged. The solute−water interaction energy also decreases markedly at this point as one of the faces of each plate is no longer exposed to the water molecules at $r_0 = 6.0$ Å and thereby decreases the total number of water−solute interactions. The decrease in the water−solute interaction energy is consistent with the interaction energy (U_{conf}) of the two plates with ∼14 water molecules in the confined region at $r_0 = 6.2$. The undulating values of the U_{conf} as listed in Table 1 are also in accord with the undulating structure of the PMF.

The hydrogen bond density profile at $r_0 = 6.8$ is shown in Figure 5a. For the case where there is but a single layer of water, the number of hydrogen bonds per water molecule n_{HB} is around 2.9 in the confined region as compared to ∼3.5 in the bulk region far away from the plates. While one might have expected less, this is reasonable in light of two hydrogen bonds being seen in the one-dimensional case of nanotubes.[23,24] Although the energy cost due to the reduction in the number of hydrogen bonds does not favor the formation of a monolayer, the stability of the water monolayer in the present case can easily be explained from the gain in favorable energy due to solute−solvent interactions. The average loss of 0.5 to 0.6 hydrogen bonds amounts to an energy cost of −6 kJ/mol (considering the H-bond energy to be −10 kJ/mol[66,67]) which is more than compensated by the gain in the van der Waals interaction energy (−10.02 kJ/mol) of water with the carbon atoms of the two

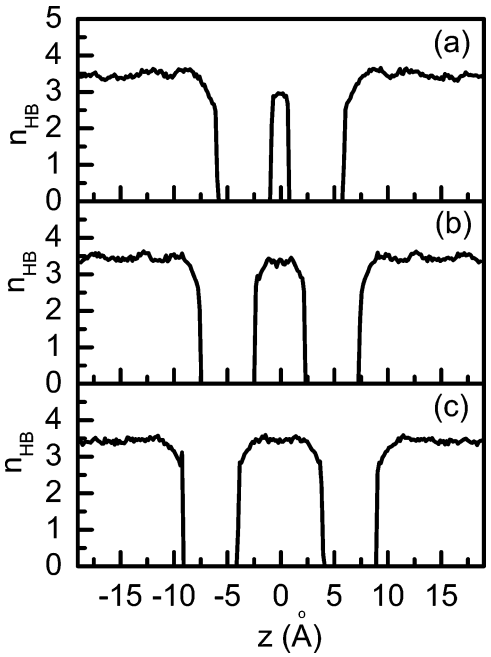

Figure 5. Number of hydrogen bonds (n_{HB}) per water molecules as a function of z for the type I solute−water system with interplate separations of (a) 6.8 Å, (b) 9.8 Å, and (c) 13 Å.

plates. The stability of the confined water in lower dimensions is also due to a sharp distribution of the water molecule around intermediate binding energies as compared to a much flatter distribution covering both high and low binding energy states for bulk water, as noted by Hummer et al.[23] A mean field theory has recently been developed[68] to study phase transitions in water films confined between two infinite walls. That theory predicted that replacement of the hydrogen bonding interactions with attractive solute−water interactions could lead to the thermodynamic stability of the water film that would otherwise have evaporated between two purely repulsive walls.

In Figures 5b and c, we plot the hydrogen bond density profiles for $r_0 = 9.8$ Å and $r_0 = 13$ Å corresponding, respectively, to two and three intervening water layers. Although the overall shape of the profile is the same in all the three cases, the number of hydrogen bonds in the confined region increases with increasing values of r_0. The value of n_{HB} in the confined region for the interplate separation $r_0 = 13$ Å reaches almost the bulk value of 3.5.

2. Type II System. To investigate the role of the nature of the solute−solvent interaction on the PMF as well as on cavitation or drying phenomena, we have considered hydrophobic plates, which are geometrically the same as the type I solute but made up of carbon atoms modeled with a purely repulsive interaction instead of weakly attractive LJ interaction considered in the case of type I solute. As already mentioned, the WCA decomposition scheme is used to split the LJ potential of type I solute into attractive and repulsive parts, and only the repulsive part is used for the type II model. The change in Gibbs' free energy $w(r)$ as a function of the distance between the two purely repulsive hydrophobic plates of type II is shown in Figure 1b along with the solute−solute potential contribution $U_{gg}(r)$ and the solvent contribution $w_{sol}(r)$ to the PMF. As in the

(66) Roberts, J. A.; Zhang, X.; Zheng, Y. *J. Chem. Phys.* **1994**, *100*, 1503.
(67) Silverstein, K. A. T.; Haymet, A. D. J.; Dill, K. A. *J. Phys. Chem. B* **2003**, *107*, 11742.
(68) Truskett, T. M.; Debenedetti, P. G.; Torquato, S. *J. Chem. Phys.* **2001**, *114*, 2401.

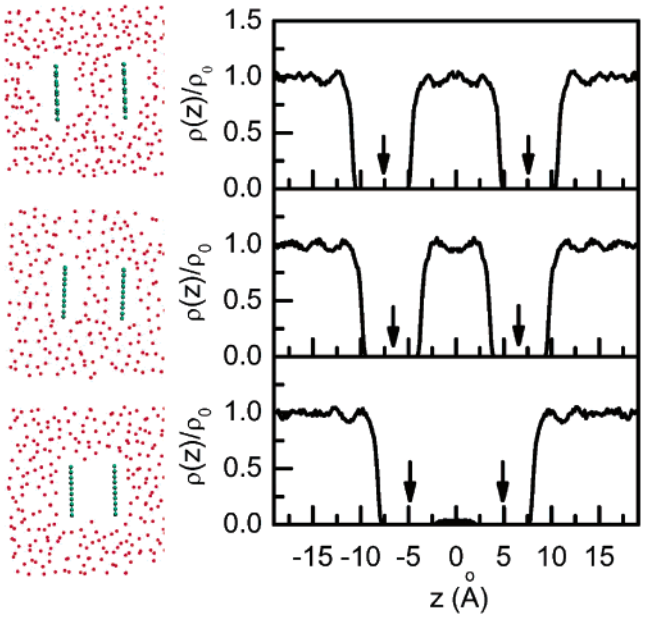

Figure 6. Type II solute−solvent distributions. (Left) Plot of a configuration for the system with type II solutes with the interplate separations (top) $r_0 = 15.4$ Å, (middle) $r_0 = 13.4$ Å, and (bottom) $r_0 = 10$ Å. Legend is same as in that in Figure 2. (Right) Plots of the normalized single particle density $\rho(z)/\rho_0$ vs z corresponding to the systems on the left.

previous case, at large separations there are shallow local minima in the PMF corresponding to integral numbers of intervening water layers. Both the coordinates and density profile corresponding to the minimum at around $r_0 = 15.4$ Å reveal (see top panels of Figure 6) roughly three intervening water layers, while those corresponding to the minimum at $r_0 = 13.4$ Å show (see middle panels of Figure 6) two intervening water layers. However, the peaks between the plates as well as adjacent to the outer surface of the plates are not as sharp and strong as those in the case of type I solute with LJ interaction. This is reminiscent of previous observations.[16,26] We do not consider this effect at this distance to be microscopic dewetting but to be related to the coordination of a loose tetrahedral network with a distinct, characteristic orientational probability as is often seen around hydrophobic atoms in contrast with those which have more attraction for the solvent.[69]

As noted above, the PMF in this case is significantly different from that of type I solutes below the intersolute separation of around 10 Å. A monotonic linear decrease in the free energy change below $r_0 \approx 12$ Å is observed in the present case. Comparison of the solvent contribution to the PMF in the present type II case with that of type I solute near the contact minimum reveals that the mechanisms of stabilization of the contact configuration is strikingly different between these two types of solutes as already mentioned. The major stabilizing contribution to the free energy at contact comes from the solute−solute interactions in the type I case, while indirect solvent induced interaction is the dominating contribution in the repulsive solute case.

The examination of the coordinates and the density profile at $r_0 = 10$ Å as shown in the two plots at the bottom of Figure 6 reveals that there are no water molecules between the two plates. In the present case we do not observe any layers of water

(69) Makarov, V. A.; Andrews, B. A.; Pettitt, B. M. *Biophys. J.* **1998**, *74*, 413.

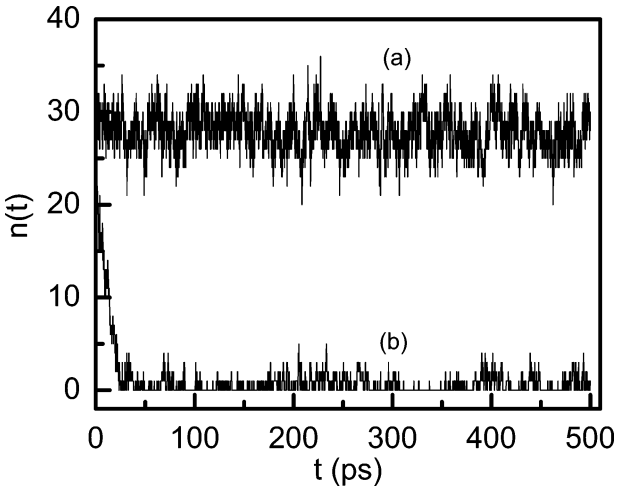

Figure 7. Plot of the number of confined water molecules $n(t)$ between the two plates vs time in picoseconds at the interplate separation of 10 Å for the systems with (a) type I solutes and (b) type II solutes in water.

between the two plates, although there is sufficient space between the two plates to fit about a couple of layers of water. Once the cavity is formed between the two plates (at $r_0 < 10$ Å), for a fixed solute size, the area of the liquid−vapor interface of the cavity is directly proportional to the interplate separation r_0 by model construction. In this regime, however, the contact area between the plates and water remains constant. Thus both surface area and the volume are linear functions of r_0. The change in the free energy in this regime is thus expected to decrease linearly with the decrease in r_0 and hence the area (ΔA) of the interface between vacuum and liquid water, and thus one has the relation

$$\Delta G = \gamma_{lv} \Delta A \tag{7}$$

where γ_{lv}, the liquid−vapor surface tension, is the constant of proportionality. In fact, examination of the free energy change computed from the present simulation shows a linear decrease with decreasing r_0 below 10 Å, and the constant attractive force in this regime amounts to around 20.08 kJ/mol/Å giving rise to a liquid−vapor surface tension of 0.43 kJ/mol/Å (or 71.7 mJ/m^2). The good agreement of this estimated γ_{lv} with the $\gamma_{lv} = 73.6$ mJ/m^2 reported[14] recently for the water−vapor interface of the SPC/E water model indicates that the expulsion of water from the confined region between the two purely repulsive plates of type II below the interplate separation of 10 Å creates a vacuous bubble, and the free energy cost of maintaining the interface strongly resembles that of the free planar water−vapor interface.

In Figure 7, we have shown the number of water molecules $n(t)$ between the two plates as a function of time for $r_0 = 10$ Å starting from the point at which the attractive potential was removed. For comparison, in the same figure we have also shown $n(t)$ at same r_0 but with the full LJ interaction (type I solute). We started the type II simulation with a configuration from the type I simulation where there were around 25−30 water molecules between the two plates. As it is seen in Figure 7, within ~50 ps, almost all the water molecules are expelled from the confined region in the case of type II solute (Figure 7b), while, in the case of type I solute, there are around 25−30 molecules present throughout the entire time period of 500 ps (Figure 7a). The response of the system to this dewetting or

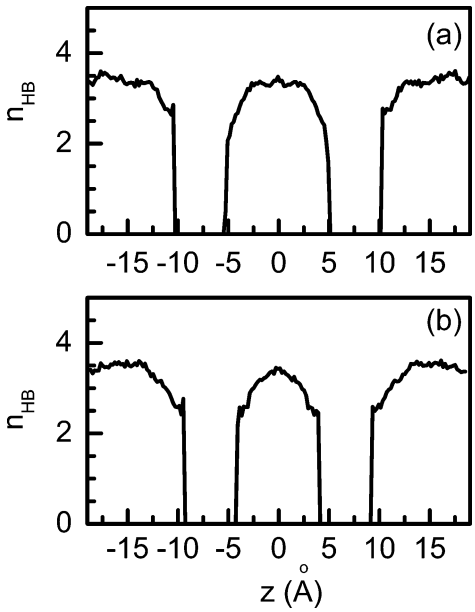

Figure 8. Number of hydrogen bonds (n_{HB}) per water molecules as a function of z for the type II solute−water system with interplate separation of (a) 15.4 Å and (b) 13.4 Å.

cavity forming phenomena is manifested by the increase in average volume of the simulation cell from $V = 57.3$ nm^3 at $r_0 = 13.4$ Å to $V = 58.5$ nm^3 at $r_0 = 10$ Å and also by the decrease of solute−solvent potential energy from 27.27 kJ/mol at $r_0 = 13.4$ Å to 18.77 kJ/mol at $r_0 = 10$ Å due to unavailability of the inner surfaces of the plates to the water molecules. The increase in volume can easily be accounted for by calculating the volume required to accommodate around 30 water molecules in the bulk corresponding to the density of 0.99 g/cc.

The hydrogen bond density profile for the systems with $r_0 = 15.4$ and $r_0 = 13.4$ corresponding to three and two intervening water layers are shown in Figure 8a and b, respectively. In both of the cases the number of hydrogen bonds n_{HB} per water molecule in the middle of the confined region is almost the same as the bulk value, although there is a significant depletion in n_{HB} around hydrophobic plates compared to Figure 5. However, when the distance between the plates are reduced from 15.4 to 13.4 Å (compare Figure 8a and b), the range of this depleted region increases and thus destabilizes the system and the potential for maintaining layers on further reduction in the interplate separation. If we assume that the reduction in the n_{HB} in going from bulk water to the monolayer state is the same as in the earlier case (type I solute case), the lost energy due to this reduction in n_{HB} is not compensated by the solute−solvent interaction as this interaction is repulsive or, at best, zero in this case.

B. Orientational Structure of Water. The orientational structure of the water molecules can be considered by calculating two orientational probability distributions $P_\mu(\cos\theta)$ and $P_{OH}(\cos\theta)$ of the water with the plate. In $P_\mu(\cos\theta)$ the angle θ is that between the dipole moment vector μ of water and the outward normal from the nearest plate pointing into the water. In the case of $P_{OH}(\cos\theta)$ the angle is that between the OH bond vector and the outward normal from the nearest wall pointing into the water. To observe how model water molecules orient themselves adjacent to the plate as well as away from it, we have divided the slab of water into five different layers.

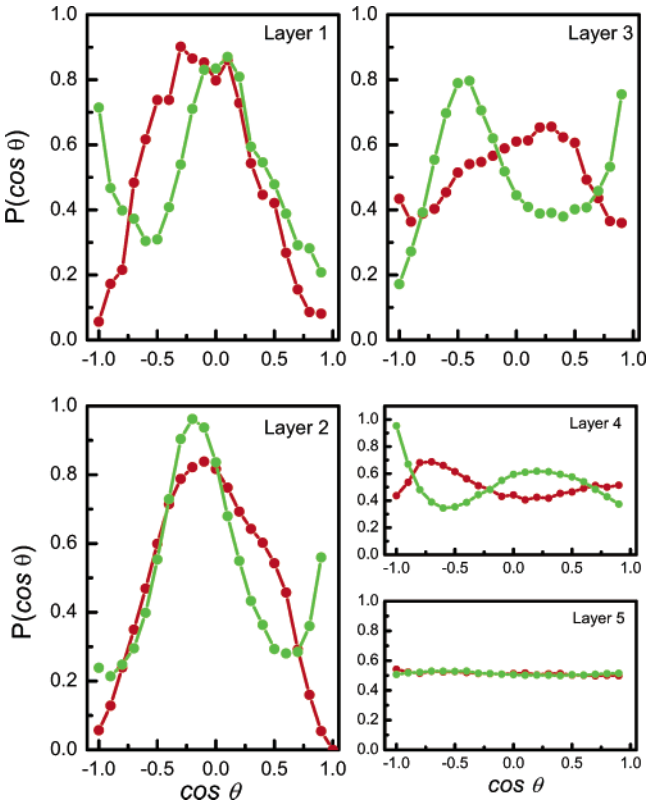

Figure 9. Orientational distribution $P(\cos\theta)$ vs $\cos\theta$. Red curves represent the angular distributions of the dipole vectors of the water molecules, while the green curves represent the distributions of the OH bond vectors. In both of the cases angle θ is defined as that between the vector (either dipole or OH bond) and the normal drawn from the nearest solute plate into the water. Layers 1−5 represent five different layers of water moving away from the outside surfaces of the solutes (discussed in the text).

Layer 1 is considered to be the layers of water molecules nearest to the outside surfaces of the plates, and it essentially contains the water molecules which reside in the repulsive region of the plate−water potential corresponding to the low-density edges before the first density maximum of the density profile. Layer 2 incorporates the molecules in the first major density maximum, while layer 3 incorporates the trough between first and second density peaks and layer 4 is the region where we have second density maximum. The region beyond the second density maximum where the density distribution reaches almost the bulk value is considered as layer 5. The distributions for the water molecules inside the two plates have not been calculated here.

The results for $P_\mu(\cos\theta)$ for the five layers of the water in system I with $r_0 = 6.8$ Å are shown as red lines with symbols in Figure 9. Near the hydrophobic surface (layers 1 and 2) we have a peak in the distribution around $\theta = 90°$ suggesting that dipoles prefer to avoid the surface normal direction. This result is consistent with the earlier studies of water between two infinite hydrophobic walls.[16,17,70] In layer 5, we observe a flat distribution of almost constant value of 0.5, characteristic of a homogeneous fluid. In layers 3 and 4 dipoles are distributed in almost opposite fashion, although the distribution for layer 4 is flatter, indicating that this region too is close to homogeneous.

In the same figure we show the $P_{OH}(\cos\theta)$ distributions for five different layers of the same system with $r_0 = 6.8$ Å as shown by the green lines and symbols. The distribution in layer

(70) Shelley, J. C.; Patey, G. N. *Mol. Phys.* **1996**, *88*, 385.

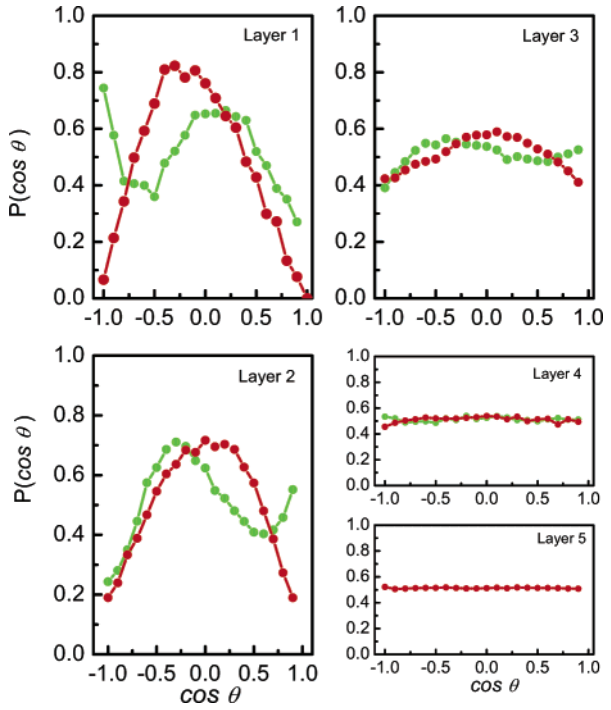

Figure 10. Same as Figure 9 but for type II solutes.

1 indicates that a large fraction of water molecules orient themselves with one OH bond pointing directly toward the hydrophobic surface as seen in the earliest simulations of Rossky.[16] There is also another peak around 90°. The distribution at layer 3 is almost opposite to that of layer 1. Although layers 1 and 3 correspond to the low-density regions due to the repulsive plate−water and water−water potential, respectively, the orientations of water molecules near hydrophobic plates (layer 1) seem to be different from the orientations near another water layer (layer 3) due to the possibility of interlayer hydrogen bonding in the latter case. The orientations in layer 2 corresponding to the first density peak show a strong distribution around θ slightly less than 90°. The distribution in layer 4, which encompasses the second density peak, has a peak at around 180°, while layer 5 shows that water molecules in this region are as random as in the bulk.

We now compare this with the angular distributions for type II solutes using the same criteria as above. The plots for $P_\mu(\cos\theta)$ and $P_{OH}(\cos\theta)$ at $r_0 = 10$ Å are shown by the red and green lines and symbols, respectively, in Figure 10. Qualitatively both $P_\mu(\cos\theta)$ and $P_{OH}(\cos\theta)$ for each individual layer are similar to the corresponding distribution for the type I solute (shown in Figure 9). Similar observation has been made earlier[71] for the orientation of the water molecule around a neopentane molecule. Quantitatively, we observe a somewhat less intense distribution in the present case as compared to the earlier case indicating that water molecules are not quite as structured orientationally in the case of repulsive solutes. This is evident if we compare layers 3 and 4 in the two cases for both of the orientational distributions. For type II solutes these distributions have almost reached the homogeneous limit. Thus, orientation of the water molecules near the nanoscopic solute surface does not change much with the change in the water−solute interaction from weakly attractive to purely repulsive. It

(71) Huang, X.; Margulis, C. J.; Berne, B. J. *J. Phys. Chem. B* **2003**, *107*, 11742.

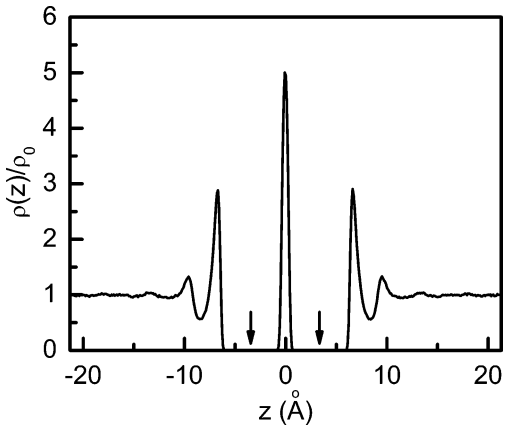

Figure 11. Normalized single particle density $\rho(z)/\rho_0$ as a function of z for the system with larger plate size of 20 Å × 20 Å at an interplate separation of 6.8 Å.

should be noted in this context that a lack of a strong sharp peak in the water density distribution near the wall does not mean a lack of orientational ordering near the wall.[16]

C. Size Effects. To investigate the effect of size of the planar solute on the dewetting transition, we have simulated additional larger type I systems and smaller type II systems. For the type I system we held the geometry at $r_0 = 6.8$ Å with two larger plates of size ~20 Å × 20 Å in water (180 carbon atoms each). The plot of the density profile for this system is shown in Figure 11. A sharp peak between the two plates in the density profile indicates that there is no dewetting with this larger solute. The same peak height outside the walls in this case as those obtained from the smaller 11 Å × 12 Å solute (see Figure 2c) indicates that there is essentially no observable density depression with this larger solute. Thus, the somewhat smaller 60 atom plates seem to capture the same effects.

To check the size response to dewetting, we have performed an additional type II simulation of 1 ns for $r_0 = 10$ Å with much smaller plates, each with the dimensions of around 7 Å × 7 Å having only 28 carbon atoms with repulsive interactions. The result for the density distribution is shown in Figure 12a. For comparison, in the same figure we have also included the density profile for the larger solute (type II) at the same r_0. For smaller solutes we observe a significant number of water molecules between the two plates as indicated by the peak in the middle of the density profile, whereas no significant density peak was observed in the case of larger solutes at the same distance as shown by the black line. The instantaneous change in the number of water molecules inside the two smaller plates has also been shown in Figure 12b for 1 ns. It is interesting to observe that although most of the time there are around 5−10 water molecules in the confined region, water gets expelled from the region and again reenters the region with the passage of time. Thus, there is a strong size dependence on dewetting for repulsive (nonphysical) solutes as predicted.[12,13]

The emptying and filling of a hydrophobic pore has been observed[23,25,72] earlier in case of carbon nanotube. For the repulsive small plates the fluctuation in the number of water molecules in the confined region becomes large. This size of the solute thus may be near the critical size above which

(72) Kalra, A.; Garde, S.; Hummer, G. *Proc. Natl. Acad. Sci. U.S.A.* **2003**, *100*, 10175.

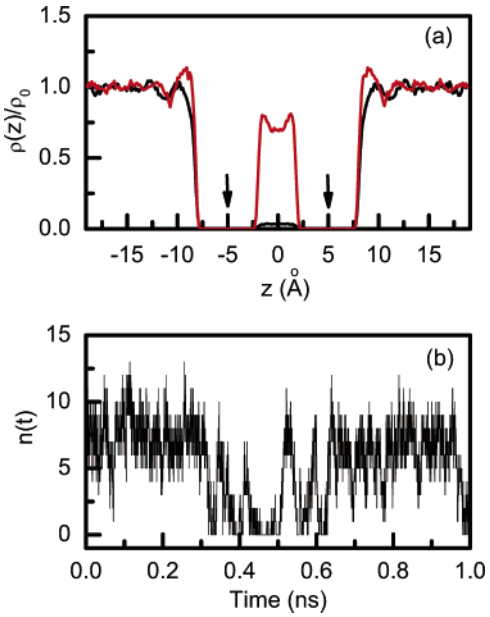

Figure 12. (a) Plot of the normalized single particle density $\rho(z)/\rho_0$ vs z for a system with smaller (~7 Å × 7 Å) (red) and larger (~11 Å × 12 Å) (black) sizes of the type II plates at an interplate separation of 10 Å and (b) plot of the number of confined water molecules $n(t)$ between the two plates vs time in nanoseconds for the system corresponding to red curve in Figure 12a.

dewetting will be observed for soft repulsive potentials for planar solutes with atomic features in SPC/E water.[12]

We conclude that cavitation or the drying transition depends not only on the size of the solute but also strongly on the nature of the interaction of the solute with water. When solute size is small, irrespective of the nature (whether attractive or repulsive) of the interaction between solute atom and solvent, water molecules are able to rearrange themselves to restore, at least in part, the hydrogen bond network without creating any dry cavity. For a large size hydrophobic solute, however, a fine balance among solute−solvent and solvent−solvent interactions and hydrogen bonding energies is required to determine whether cavitation or strict microscopic dewetting will occur.

IV. Conclusions

The mechanism of the hydrophobic effect thus changes with respect to solute size and the nature of the interactions in a regular and explainable fashion. The potentials of mean force between two nanoscopically large planar solute plates made up of model, hydrophobic carbon atoms placed in a hexagonal graphitelike lattice with two different types of interaction potentials are quite revealing.

Comparison of the solvent contribution to the PMFs near the contact minimum reveals that the mechanisms of stabilization of the contact configuration are strikingly different between the two types of solutes. The major stabilizing contribution to the free energy at contact comes from the solute−solute interactions in the type I case, while indirect solvent induced interaction is the dominating contribution in the repulsive solute case. The attractive type I plates show a significant solvent induced barrier to dissociation, whereas the repulsive plates show hardly any barriers.

In the case of solute atoms interacting through usual LJ interaction (type I), we do not observe any cavitation or dewetting until the distance between the two plates is less than the onset of steric hindrance which prevents water molecules from staying between two solutes near standard temperatures and pressures. Even if the sizes of the solute plates are roughly 20 Å on a side, no cavitation is observed for this interaction potential. Interestingly, if we consider the solute−water interaction to be a purely repulsive one (type II solute), we observe a profound dewetting below an intersolute separation of ~10 Å, although water layers between the two solute plates at this separation could be easily accommodated from the excluded volume consideration. By changing the solute size to a smaller one in this case, we do not observe any dewetting or cavitation as is the case for type I solutes. This shows that the gross hydration behavior of the small solutes does not depend much on the nature of weak solute−solvent attractive interactions.

For larger solutes, however, hydration behavior more strongly depends on the nature of the solute−solvent interaction. In the case of solutes with a slight attractive interaction, water molecules strongly hydrate the solutes and also enter a narrow confined region of width 6.8 Å between the two solutes irrespective of the lateral extent of the planar solutes studied here. On the other hand, when a purely repulsive interaction energy is considered between the solute atoms and the water, hydration behavior clearly depends on the solute size. The present investigation shows that the tendency toward cavitation between the plates depends on the attractive nature of the solute−water interaction (as well as size) and thus explains many of the differences in previous literature results regarding wetting or dewetting. We make no claim here about the nature of the actual graphitic carbon−water potential. Indeed there could be significant polarizability effects beyond mean field for an amphoteric substance like graphene sheets.

Several important questions were recently raised in the literature[20] about the effect of attractive solute−water interactions on observed dewetting. As speculated there we find the large number of small water−solute attractive interactions can compensate for the loss of hydrogen bonds due to confinement of water between the two plates. A detailed quantitative understanding of solute−water attractions is thus required to predict dewetting induced aggregation of complex biomolecules. A recent work by Berne and coworkers[73] demonstrated that simulations of proteins show a sensitivity to the attractive interactions with water, and they confirmed that without van der Waals and electrostatic interactions the core dewetting and collapse are on a substantially different time scale. As even the most hydrophobic regions in proteins have weak polarity and significant dispersion interactions, our present investigation shows the importance of taking into consideration such interactions in dealing with hydrophobicity induced aggregation and folding of proteins. The type I parameters we have used are of the order of magnitude found in a variety of common force fields. We also investigated solute−solvent attractions considerably smaller than those routinely used to investigate the physical properties of carbon and found even quite weak Lennard−Jones attractions significantly change the hydration behavior from dewetting to wetting. This level of detailed understanding of the influence of individually small (less than kT) direct interactions on the collective, indirect, solvent mediated forces may be expected to be important in the development of better force fields.

(73) Zhou, R.; Huang, X.; Margulis, C. J.; Berne, B. J. *Science* **2004**, *305*, 1605.

Acknowledgment. We thank G. C. Lynch and K.-Y. Wong for many valuable technical discussions and L. R. Pratt and A. D. J. Haymet for stimulating conversations. We gratefully acknowledge the NIH, the R.A. Welch Foundation, and TiiMES, funded by NASA Cooperative Agreement No. NCC-1-02038 for partial financial support of this work. The computations were performed in part using the NSF meta center facilities and the Molecular Science Computing Facility in the W.R. Wiley Environmental Molecular Sciences Laboratory, a national scientific user facility sponsored by DOE's Office of Biological and Environmental Research and located at Pacific Northwest National Laboratory, operated for the DOE by Battelle.

JA0441817